Integrated Sideband-Resolved SERS with a Dimer on a Nanobeam Hybrid

Ilan Shlesinger,[1] Isabelle M. Palstra,[2,1] and A. Femius Koenderink[1,2,*]
[1]Department of Physics of Information in Matter and Center for Nanophotonics, NWO-I Institute AMOLF, Science Park 104, NL1098XH Amsterdam, Netherlands
[2]Institute of Physics, University of Amsterdam, NL1098XH Amsterdam, Netherlands

(Received 30 August 2022; accepted 14 December 2022; published 6 January 2023)

In analogy to cavity optomechanics, enhancing specific sidebands of a Raman process with narrowband optical resonators would allow for parametric amplification, entanglement of light and molecular vibrations, and reduced transduction noise. We report on the demonstration of waveguide-addressable sideband-resolved surface-enhanced Raman scattering (SERS). We realized a hybrid plasmonic-photonic resonator consisting of a 1D photonic crystal cavity decorated with a sub-20 nm gap dimer nanoantenna. Hybrid resonances in the near-IR provide designer Q factors of 1000, and $Q/V = (\lambda^3/10^6)^{-1}$, with SERS signal strength on par with levels found in state-of-the-art purely plasmonic systems. We evidence Fano line shapes in the SERS enhancement of organic molecules, and quantitatively separate out the pump enhancement and optical reservoir contributions.

DOI: 10.1103/PhysRevLett.130.016901

Molecules can exchange energy with incident light through the vibrations of their atomic bonds [1], giving rise to inelastic light scattering, called Raman scattering. Surface-enhanced Raman scattering (SERS) uses plasmonic nanoparticles featuring intense field hot spots to enhance the intrinsically weak Raman scattering of molecules by orders of magnitude, and is among the most popular single-molecule sensitive spectroscopy tools [2–5]. Recently, theoretical efforts have sought to exploit formal analogies between SERS and cavity optomechanics [6–10], which is the field of precisely controlling and sensing the mechanical motion of nano- and microresonators with light. The molecular optomechanics viewpoint promises to bring the exciting effects that were obtained in nanoengineered MHz/GHz acoustic resonators, such as strong optomechanical coupling, production of nonclassical mechanical states, parametric amplification, and coherent wavelength conversion [11,12], to THz and mid-IR molecular vibrations. The two latter have recently been demonstrated with molecules [9,13,14], and collective effects in Raman scattering have also been observed [15,16].

A central tenet of cavity optomechanics is that so-called sideband-resolved operation is crucial, which is attained when the optical cavity has a linewidth smaller than the mechanical resonance frequency [11,12]. It eliminates detrimental backaction, thus allowing ground-state cooling, pure light-mechanical entanglement, and frequency conversion without added noise. High-quality factor (Q) dielectric cavities can provide the narrow band spectral structure required for sideband-resolved SERS, but are limited to low electric field confinement, resulting in small optomechanical coupling strengths and very low Raman enhancement compared to plasmonic systems. Conversely, the optical linewidth ($Q = 10$–30) for typical plasmon antennas [17]) exceeds the vibrational frequencies, so that established SERS geometries are not sideband resolved. A major challenge lies in reaching sideband resolution while maintaining the uniquely strong field enhancement of metal junctions. Furthermore, a significant open question for both traditional SERS and prospective molecular sideband-resolved optomechanics is how to achieve waveguide addressability. All SERS demonstrations with few molecules have been limited to free-space configurations, since integrated geometries are rapidly confronted by high background noise emanating from the guiding material [18,19].

In this Letter, we report on the realization of a proposed new generation of hybrid light resonators [20–22] that combine a plasmonic antenna interacting with a dielectric cavity and features narrow and intense resonances [23–25]. We show how it allows for few-molecules sideband-resolved SERS with selective enhancement of single Raman lines and with waveguide excitation and collection capabilities (Fig. 1). The system combines photonic crystal nanobeam cavities [26] with single gold dimer antennas [27], aligned within a few nanometers by two-step lithography. The hybridization of a broad plasmonic resonance with the sharp cavity peak results in sharp Fano features in the optical reservoir [28,29], i.e., in the local density of optical states (LDOS) landscape felt by the Raman species with which we functionalized the gold antennas. We present a study using a confocal Raman spectroscopy setup [see Supplemental Material (SM) [30]] with a tunable laser, disentangling the role of pump enhancements and the LDOS landscape, and evidencing waveguide-addressed sideband-resolved SERS.

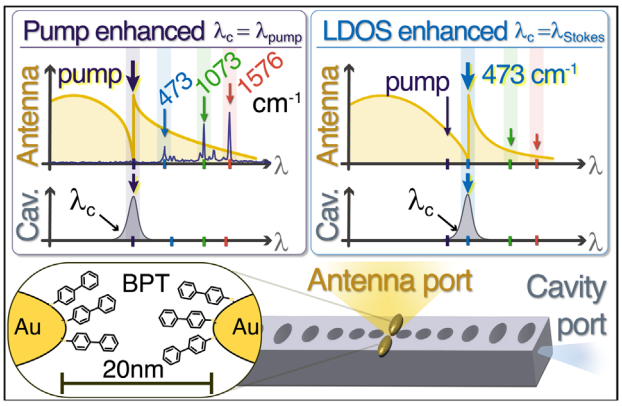

FIG. 1. A gold dimer antenna, decorated with BPT molecules, hybridizing with a Si_3N_4 photonic crystal nanobeam. Depending on the cavity resonance wavelength, either the pump (left) or a single BPT Raman peak (right) is enhanced by the hybrid resonance. The enhancement line shape will depend on the addressed optical port, featuring a Fano line shape for the antenna or a Lorentzianlike shape for the cavity.

SEM micrographs in Figs. 2(a) and 2(b) show a representative example of a hybrid composed of a gold dimer antenna with a 20 nm gap placed on top and in the center of a Si_3N_4 photonic crystal lying on a SiO_2 layer (see SM for design and fabrication details [30]). Two gratings on each side of the nanobeam allow coupling light from free space to the waveguide. While the aligned multistep electron-beam lithography required to realize these samples is challenging, the robustness of our fabrication protocol is evident from the fact that our study is based on optical measurements on over 280 of such hybrid resonators. Design quality factors predict $Q_c \simeq 2500$ and mode volumes $V_c \sim 3\lambda^3$ for the nanobeam and $V_a = 10^{-4}\lambda^3$ for the dimers, resulting in $Q \sim 10^3$ and $V \sim 2 \times 10^{-3}\lambda^3$ for hybrids [21]. The resulting Q/V ratio of 10^6 in units of $1/\lambda^3$ is on par with state-of-the-art plasmonic resonators [38] and photonic crystal cavities [26], but with the unique asset that Q can be chosen at will from 10^2 to 10^3.

The first experimental signatures of hybridization are readily observed in the spatial scattering of the cavity presented in Figs. 2(c) and 2(d). In panels (d) and (e), a tunable diode laser, resonant with the cavity (ca. 780 nm), is aimed at the left incoupling grating, just outside the field of view. For the hybrid system, there is bright scattering from the antenna [bright dot in (d); the antenna appears as a dark spot in bright-field microscopy (c)]. On the contrary, in absence of an antenna, the light is mainly outcoupled from the second grating [Fig. 2(e)]. This shows that it is possible to drive the gold dimer antenna through the nanobeam structure, implying optical coupling between the cavity and the plasmon resonances. This coupling provides frequency structure in hybrid LDOS enhancement and waveguide addressability of the plasmonic hot spot.

Figures 3(a) and 3(b) report on the measured optical resonance properties of the individual constituents, that is, antenna and cavity, and of the hybrids. Bare antenna darkfield (DF) spectra confirm that the dimer antennas feature a dipolar resonance with $Q \sim 10$ and polarized

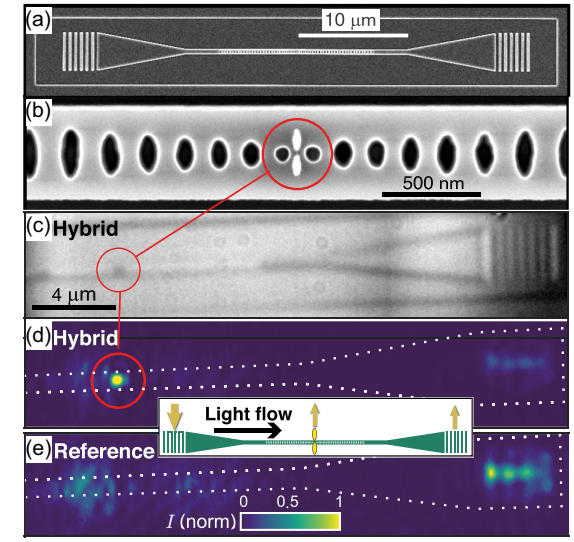

FIG. 2. (a) SEM micrograph of a nanobeam cavity with grating couplers on each side. (b) Aligned dimer antenna placed on top and in the center of the cavity. (c) Bright-field white-light (WL) microscopy image showing the cavity (left-hand part of figure) and grating outcoupler (right-hand side). The antenna appears as a black dot. (d) Laser scattering of the same device and (e) a device with no antenna. The system is driven by a laser resonant with the cavity, and focused on the left incoupling grating (not visible here). Bright scattering by the antenna demonstrates antenna-cavity coupling.

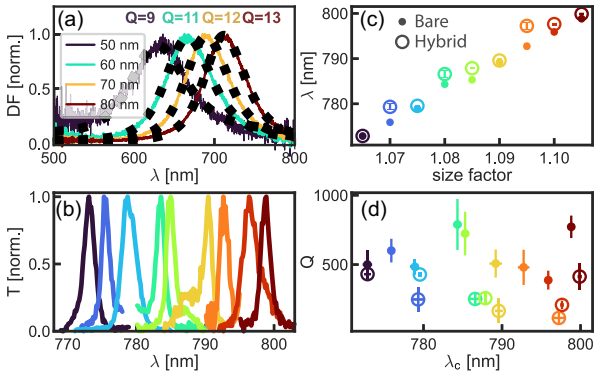

FIG. 3. (a) DF spectra of bare gold dimers. Resonances redshift with antenna size. Q's are extracted from squared Lorentzian fits (dashed lines). (b) Transmission of the bare nanobeam cavities, nine different designs were made with four devices studied per design. Increasing the in-plane photonic crystal hole radius and period (scaling parameter on x axis) tunes the cavity resonance (c). In the presence of the antenna, the hybridized cavity mode is redshifted and broadened (open circular markers) (c) and (d). Error bars are standard deviations from four different but nominally identical beams or hybrids.

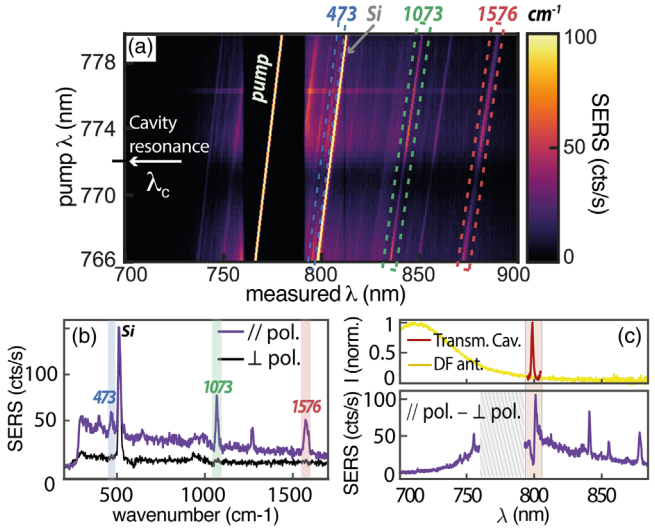

FIG. 4. (a) SERS on a hybrid for pump wavelengths scanned from 766 to 780 nm. The Fano response of the hybridized antenna can be seen as a lowering and raising of SERS intensity when passing through the cavity resonance frequency (pump enhancement effect, near 772 nm). (b) Cross-cut of (a) for $\lambda_{\mathrm{pump}} =$ 774 nm (purple line). Raman scattering from the BPT is only detected when the laser is polarized parallel to the dimer. For orthogonal polarization, only the Si signal from the substrate is seen (black curve). (c) DF and transmission spectrum of a hybrid where the cavity resonance at 800 nm lies in the Stokes sideband (LDOS enhancement). Bottom: SERS spectrum featuring a clear Fano resonance at the hybrid resonance (silicon background subtracted).

along their long axis. Figure 3(b) shows transmission spectra of antenna-free nanobeam cavities. The resonance wavelength can be tuned from 772 to 800 nm by changing the position and width of the holes by 4% size difference [Fig. 3(c), full dots]. As shown in Fig. 3(d) in closed symbols, the bare cavity modes have measured $Q \sim 600$ with strong variability due to fabrication imperfections, and with the highest values obtained equal to $Q \simeq 1000$. The parameters of the hybridized cavity with the antennas are shown with circled markers. Although the spread in the nanobeam cavity resonance wavelength λ_c and Q due to fabrication fluctuations makes it difficult to directly measure cavity perturbation effects by comparing different devices, we find that hybridized resonances appear systematically redshifted and broadened compared to bare cavities, as expected from cavity perturbation theory [39], with a reduction in Q towards the 200–300 range. These Q, corresponding to ca. 65 cm^{-1} linewidths, are ideally suited for sideband-resolved SERS: sufficiently narrow to select single low frequency vibrational lines, yet wide enough to encompass typical Raman linewidths in full [1].

To this end, we functionalize the antennas with biphenyl-4-thiol (BPT) molecules which form self-assembled monolayers on gold, and exhibit distinct Raman scattering [30,40]. Figure 4(a) shows a set of Raman spectra recorded on a hybrid as a function of both detection wavelength and pump wavelength. Here, excitation and collection are done through the antenna port and the laser is polarized parallel to the dimer long axis. As the pump laser is swept from 766 to 780 nm (residual transmitted pump light through the notch filter visible), the BPT Raman lines (lines of interest highlighted in dashed boxes) maintain a constant shift from the laser frequency. In Fig. 4(a) the cavity resonance lies at 772 nm. While scanning the laser through that wavelength, the hybrid Fano response of the antenna at the cavity frequency results in a Fano shaped pump enhancement, reducing the pump field enhancement at the Fano dip around 771 nm and increasing it at the Fano peak around 774 nm. The intensity of the electronic Raman scattering [41] (broad Raman background) and the narrow BPT Raman peaks show this trend in the pump enhancement, most noticeably as the dark region around 771 nm. Instead, the silicon peak (bright line at 520 cm^{-1}) emitted by the underlying substrate has a constant intensity, evidencing that the signal modulation is actually due to the hybrid resonance and not to an overall change in pump laser intensity. To confirm that the SERS signal comes strictly from BPT molecules at the antenna, we plot in Fig. 4(b) a cross-cut of the Raman spectrum recorded at $\lambda_{\mathrm{laser}} =$ 774 nm (purple line) and a reference case with pump polarization orthogonal to the antenna long axis (black line). A SERS signal is observed only for the parallel case. In the orthogonal configuration no BPT Raman peaks appear and only the Raman line from the silicon substrate is observed. The intermediate glass and PMMA cladding do not contribute to the Raman signal. Considering that the BPT counts in the reference case are below noise levels of 1 count/s, we deduce a lower bound on Raman enhancement of 1.1×10^4, limited by our 20 min integration time. The actual enhancement is estimated to be 2–3 orders of magnitude larger using a semianalytical model presented in the SM [30].

To highlight the effect of hybrid LDOS, Fig. 4(c) shows a Raman spectrum from a different hybrid with $\lambda_c = 800$ nm that now lies in the Stokes sideband. The top diagram shows the relevant antenna DF spectrum and cavity transmission. Interference of the narrow-cavity resonance and the broad dimer response results in a structured LDOS with a Fano line shape. This Fano resonance is imprinted on the broad electronic Raman scattering background of the gold, around 800 nm wavelength (bottom panel), and the Fano peak is tuned to enhance the BPT line at 473 cm^{-1}. Combined, Figs. 4(a)–4(c) qualitatively show that it is possible to superimpose the hybrid resonance selectively with either the pump wavelength or with specific Raman lines.

In Fig. 5, we quantitatively explore the SERS enhancement engineering achieved with the hybrid resonance, allowing integrated sideband-resolved SERS. First, we discuss the SERS response of hybrids resonant with the

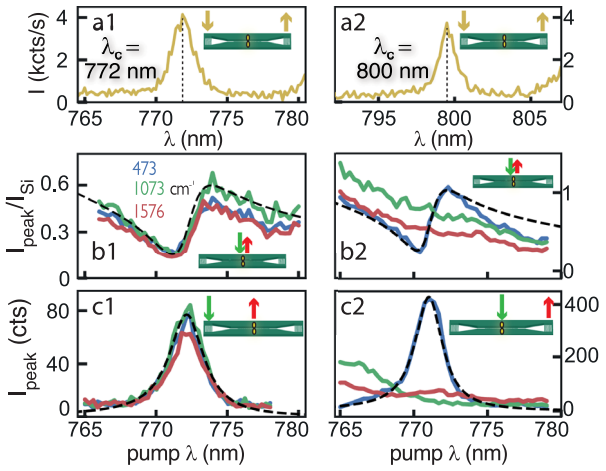

FIG. 5. Pump (left column) or LDOS (right column) hybrid enhancement. The pump (left) or the 473 cm^{-1} peak (right) are, respectively, swept through the hybrid cavity resonance. (a) WL transmission spectrum of the hybridized cavity resonance. (b),(c) Integrated counts of three selected BPT Raman peak intensities for laser wavelengths from 765 to 780 nm. In (b) pump and collection is through the antenna and normalized by the Si line, taken as reference. (c1) Coupling through one grating and collecting at the antenna and (c2) is the inversed configuration. Dashed curves are from a semianalytical theoretical model [30].

pump (panels a1–c1) with a hybrid resonance at $\lambda_c = 772$ nm [same structure as in Figs. 4(a) and 4(b)]. Panels b1 and c1 are excitation spectra reporting integrated counts of the Raman peaks at 473, 1073, and 1576 cm^{-1} (blue, green, and red curves) as a function of pump wavelength (swept from 765–780 nm at 400 μW power, 20 s integration time per data point). Figure 5(b1) is for free-space excitation and collection on the antenna. A clear Fano line shape is observed for the integrated counts of each peak as the laser is tuned over the hybrid resonance, consistent with the expectation that the SERS enhancement is the product of a pump-field enhancement factor (resonator property at the pump frequency) and LDOS enhancement at the Stokes-shifted frequency [42]. Here, the pump enhancement that is common to all three lines shows the hybrid Fano line shape, while the LDOS at the Stokes-shifted frequencies is unstructured, and is essentially in the featureless wing of the broad Lorentzian antenna resonance (as sketched in Fig. 1). The Fano line shape in the pump enhancement occurs because free-space pumping directly drives the broad antenna resonance, and its coupling to the narrow resonance appears as a transparency line [35,43]. Panel (c1) shows results on the same hybrid, but now driving directly the cavity through the waveguide, by aligning the pump to one of the gratings, but still collecting from the antenna. When we sweep the laser frequency, all three Raman lines again follow a very similar behavior, due to a strong spectral modification of the pump enhancement, yet an unstructured LDOS at the vibrational lines. Instead of a Fano line shape, the SERS enhancement now traces an almost Lorentzian resonance which reports the transfer function for the pump light from the grating coupler, via the cavity, to the antenna [see Fig. S5(b) in the SM [30]]. We now turn to the second scenario, wherein the hybrid provides selective LDOS enhancement, instead of pump enhancement (right column of Fig. 5). To this end, we select a different cavity with a longer $\lambda_c = 800$ nm. In contrast to the previous scenario, now the pump is not tuned through the hybrid resonance but through a wavelength interval blue-detuned by about 25 nm, exactly such that only the 473 cm^{-1} BPT Raman line is scanned across the hybrid resonance [same structure as in Fig. 4(c)]. The system is again first interrogated by free-space pumping and collection. In stark contrast to the earlier results, now only one Raman line shows a Fano line shape, while the other Raman lines follow a broad shoulder. Indeed, the pump field now enjoys the broadband enhancement of the antenna, without modification by the cavity mode, but the hybrid LDOS now shows a Fano line that acts only on the vibration that it is resonant with (see Fig. 1). The shoulder in the other lines is due to the typical SERS enhancement of the bare antenna, decreasing as one tunes away from resonance [44].

Finally, Fig. 5(c2) shows waveguide addressed SERS. As the photonic crystal cavity prohibits optical transport between the grating coupler and antenna except on cavity resonance, the pump is now provided from free space, while the Raman signal is collected from the outcoupling grating. When the 473 cm^{-1} peak is tuned over the hybrid resonance it shows a strong Lorentzian response whereas the 1073 and 1576 cm^{-1} lines barely pass through the waveguide. Here, the pump enhancement still originates from the broad antenna resonance, while the hybrid resonance provides both the LDOS and the collection efficiency into the waveguide required to enhance and efficiently collect only a single Raman line. Significant SERS enhancement into the cavity port concurs with the Fano dip in the free-space signal due to suppressed radiative loss. Importantly, the detected SERS counts from integrated operation are as good as for free space addressing which translates into an estimated sevenfold stronger integrated SERS enhancement than obtained for free-space addressing when taking into account the poor grating coupling efficiencies (see SM [30] for further analysis of signal levels). Comparison with a semianalytical model detailed in the SM [30], predicts a hybrid cooperativity (comparing the cavity-antenna coupling rate with the optical losses) of order 1, ensuring a good trade-off between hybrid enhancement and collection rates [21,35].

To conclude, we reported on the realization of a new generation of hybrid plasmonic-dielectric cavity resonators, with a lithographically designed gap antenna accurately coupled to a narrow linewidth photonic crystal cavity. The hybrid resonances allow one to selectively enhance and

collect single Raman lines in a guided mode, paving the way for on-chip applications of spectrometer-free, specific Raman species detection. The intense resonances obtained with the 20 nm gap modes, and the narrow linewidth obtained through hybridization with the high-Q cavity mode are particularly interesting for optomechanical strong coupling [24] and sideband-resolved molecular optomechanics. For instance, sideband resolution is highly relevant to observe parametric instabilities in the few molecule regime [9]. Achieving this regime would require further optimization of cavity fabrication to reach higher quality factors as expected for photonic crystal geometries [45]. Indeed, we estimate the optomechanical cooperativity C_m, which determines the degree of coherence of the light-vibration interaction, to be on the order of 10^{-3} for our system (see SM for details [30]). Cooperativities $C_m \gtrsim 1$ are expected for challenging but realistically achievable parameters $Q_c \simeq 5000$ and 4 nm dimer gaps.

We thank Alejandro Martínez and Ewold Verhagen for stimulating discussions. This work is part of the Research Program of the Netherlands Organization for Scientific Research (NWO). The authors acknowledge support from the European Unions Horizon 2020 research and innovation program under Grant Agreement No. 829067 (FET Open THOR).

I. S. and I. P. contributed equally to this work.

*f.koenderink@amolf.nl

[1] D. A. Long, *The Raman Effect: A Unified Treatment of the Theory of Raman Scattering by Molecules* (Wiley, Chichester, New York, 2002).

[2] M. Fleischmann, P. Hendra, and A. McQuillan, Raman spectra of pyridine adsorbed at a silver electrode, Chem. Phys. Lett. **26**, 163 (1974).

[3] D. L. Jeanmaire and R. P. Van Duyne, Surface Raman spectroelectrochemistry: Part I. Heterocyclic, aromatic, and aliphatic amines adsorbed on the anodized silver electrode, J. Electroanal. Chem. Interfacial Electrochem. **84**, 1 (1977).

[4] M. G. Albrecht and J. A. Creighton, Anomalously intense Raman spectra of pyridine at a silver electrode, J. Am. Chem. Soc. **99**, 5215 (1977).

[5] E. C. Le Ru and P. G. Etchegoin, Single-molecule surface-enhanced Raman spectroscopy, Annu. Rev. Phys. Chem. **63**, 65 (2012).

[6] P. Roelli, C. Galland, N. Piro, and T. J. Kippenberg, Molecular cavity optomechanics as a theory of plasmon-enhanced Raman scattering, Nat. Nanotechnol. **11**, 164 (2016).

[7] M. K. Schmidt, R. Esteban, A. González-Tudela, G. Giedke, and J. Aizpurua, Quantum mechanical description of Raman scattering from molecules in plasmonic cavities, ACS Nano **10**, 6291 (2016).

[8] F. Benz, M. K. Schmidt, A. Dreismann, R. Chikkaraddy, Y. Zhang, A. Demetriadou, C. Carnegie, H. Ohadi, B. De Nijs, R. Esteban, J. Aizpurua, and J. J. Baumberg, Single-molecule optomechanics in "picocavities", Science **354**, 726 (2016).

[9] A. Lombardi, M. K. Schmidt, L. Weller, W. M. Deacon, F. Benz, B. de Nijs, J. Aizpurua, and J. J. Baumberg, Pulsed Molecular Optomechanics in Plasmonic Nanocavities: From Nonlinear Vibrational Instabilities to Bond-Breaking, Phys. Rev. X **8**, 011016 (2018).

[10] M. K. Schmidt, R. Esteban, F. Benz, J. J. Baumberg, and J. Aizpurua, Linking classical and molecular optomechanics descriptions of SERS, Faraday Discuss. **205**, 31 (2017).

[11] M. Aspelmeyer, T. J. Kippenberg, and F. Marquardt, Cavity optomechanics, Rev. Mod. Phys. **86**, 1391 (2014).

[12] W. P. Bowen and G. J. Milburn, *Quantum Optomechanics* (CRC Press, Boca Raton, 2015).

[13] W. Chen, P. Roelli, H. Hu, S. Verlekar, S. P. Amirtharaj, A. I. Barreda, T. J. Kippenberg, M. Kovylina, E. Verhagen, A. Martínez, and C. Galland, Continuous-wave frequency upconversion with a molecular optomechanical nanocavity, Science **374**, 1264 (2021).

[14] A. Xomalis, X. Zheng, R. Chikkaraddy, Z. Koczor-Benda, E. Miele, E. Rosta, G. A. E. Vandenbosch, A. Martínez, and J. J. Baumberg, Detecting mid-infrared light by molecular frequency upconversion in dual-wavelength nanoantennas, Science **374**, 1268 (2021).

[15] Y. Zhang, J. Aizpurua, and R. Esteban, Optomechanical collective effects in surface-enhanced Raman scattering from many molecules, ACS Photonics **7**, 1676 (2020).

[16] V. Vento, S. T. Velez, A. Pogrebna, and C. Galland, Measurement-induced collective vibrational quantum coherence under spontaneous Raman scattering in a liquid, arXiv:2105.00213.

[17] M. Agio and A. Alù, *Optical Antennas* (Cambridge University Press, Cambridge, England, 2013).

[18] F. Peyskens, A. Dhakal, P. Van Dorpe, N. Le Thomas, and R. Baets, Surface enhanced Raman spectroscopy using a single mode nanophotonic-plasmonic platform, ACS Photonics **3**, 102 (2016).

[19] F. Peyskens, P. Wuytens, A. Raza, P. V. Dorpe, and R. Baets, Waveguide excitation and collection of surface-enhanced Raman scattering from a single plasmonic antenna, Nanophotonics **7**, 1299 (2018).

[20] Y.-F. Xiao, Y.-C. Liu, B.-B. Li, Y.-L. Chen, Y. Li, and Q. Gong, Strongly enhanced light-matter interaction in a hybrid photonic-plasmonic resonator, Phys. Rev. A **85**, 031805(R) (2012).

[21] H. M. Doeleman, E. Verhagen, and A. F. Koenderink, Antenna-cavity hybrids: Matching polar opposites for Purcell enhancements at any linewidth, ACS Photonics **3**, 1943 (2016).

[22] K. D. Heylman, N. Thakkar, E. H. Horak, S. C. Quillin, C. Cherqui, K. A. Knapper, D. J. Masiello, and R. H. Goldsmith, Optical microresonators as single-particle absorption spectrometers, Nat. Photonics **10**, 788 (2016).

[23] M. K. Dezfouli and S. Hughes, Quantum optics model of surface-enhanced Raman spectroscopy for arbitrarily shaped plasmonic resonators, ACS Photonics **4**, 1045 (2017).

[24] M. K. Dezfouli, R. Gordon, and S. Hughes, Molecular optomechanics in the anharmonic cavity-QED regime using

hybrid metal-dielectric cavity modes, ACS Photonics **6**, 1400 (2019).
[25] I. M. Palstra, H. M. Doeleman, and A. F. Koenderink, Hybrid cavity-antenna systems for quantum optics outside the cryostat?, Nanophotonics **8**, 1513 (2019).
[26] P. B. Deotare, M. W. McCutcheon, I. W. Frank, M. Khan, and M. Lončar, High quality factor photonic crystal nanobeam cavities, Appl. Phys. Lett. **94**, 121106 (2009).
[27] P. J. Schuck, D. P. Fromm, A. Sundaramurthy, G. S. Kino, and W. E. Moerner, Improving the Mismatch Between Light and Nanoscale Objects with Gold Bowtie Nanoantennas, Phys. Rev. Lett. **94**, 017402 (2005).
[28] M. Kamandar Dezfouli, R. Gordon, and S. Hughes, Modal theory of modified spontaneous emission of a quantum emitter in a hybrid plasmonic photonic-crystal cavity system, Phys. Rev. A **95**, 013846 (2017).
[29] I. Medina, F. J. García-Vidal, A. I. Fernández-Domínguez, and J. Feist, Few-Mode Field Quantization of Arbitrary Electromagnetic Spectral Densities, Phys. Rev. Lett. **126**, 093601 (2021).
[30] See Supplemental Material at http://link.aps.org/supplemental/10.1103/PhysRevLett.130.016901, for fabrication and experimental details, mode simulations versus geometry, and semianalytical line shape modeling, which includes References [31–37].
[31] W. Yan, R. Faggiani, and P. Lalanne, Rigorous modal analysis of plasmonic nanoresonators, Phys. Rev. B **97**, 205422 (2018).
[32] C. Vericat, M. E. Vela, G. Corthey, E. Pensa, E. Cortés, M. H. Fonticelli, F. Ibañez, G. E. Benitez, P. Carro, and R. C. Salvarezza, Self-assembled monolayers of thiolates on metals: A review article on sulfur-metal chemistry and surface structures, RSC Adv. **4**, 27730 (2014).
[33] A. Ahmed, K. Banjac, S. S. Verlekar, F. P. Cometto, M. Lingenfelder, and C. Galland, Structural order of the molecular adlayer impacts the stability of nanoparticle-on-mirror plasmonic cavities, ACS Photonics **8**, 1863 (2021).
[34] A. Xomalis, R. Chikkaraddy, E. Oksenberg, I. Shlesinger, J. Huang, E. C. Garnett, A. F. Koenderink, and J. J. Baumberg, Controlling optically driven atomic migration using crystal-facet control in plasmonic nanocavities, ACS Nano **14**, 10562 (2020).
[35] I. Shlesinger, K. G. Cognée, E. Verhagen, and A. F. Koenderink, Integrated molecular optomechanics with hybrid dielectric-metallic resonators, ACS Photonics **8**, 3506 (2021).
[36] R. S. Daveau, K. C. Balram, T. Pregnolato, J. Liu, E. H. Lee, J. D. Song, V. Verma, R. Mirin, S. W. Nam, L. Midolo, S. Stobbe, K. Srinivasan, and P. Lodahl, Efficient fiber-coupled single-photon source based on quantum dots in a photonic-crystal waveguide, Optica **4**, 178 (2017).
[37] E. C. Le Ru and P. G. Etchegoin, Chapter 4—SERS enhancement factors and related topics, in *Principles of Surface-Enhanced Raman Spectroscopy*, edited by E. C. Le Ru and P. G. Etchegoin (Elsevier, Amsterdam, 2009), pp. 185–264.
[38] J. J. Baumberg, J. Aizpurua, M. H. Mikkelsen, and D. R. Smith, Extreme nanophotonics from ultrathin metallic gaps, Nat. Mater. **18**, 668 (2019).
[39] H. Bethe and J. Schwinger, *Perturbation Theory for Cavities* (Massachusetts Institute of Technology, Radiation Laboratory, Cambridge, MA, 1943).
[40] C. D. Bain, H. A. Biebuyck, and G. M. Whitesides, Comparison of self-assembled monolayers on gold: Coadsorption of thiols and disulfides, Langmuir **5**, 723 (1989).
[41] J. Mertens, M.-E. Kleemann, R. Chikkaraddy, P. Narang, and J. J. Baumberg, How light is emitted by plasmonic metals, Nano Lett. **17**, 2568 (2017).
[42] J. Ye, F. Wen, H. Sobhani, J. B. Lassiter, P. Van Dorpe, P. Nordlander, and N. J. Halas, Plasmonic nanoclusters: Near field properties of the Fano resonance interrogated with SERS, Nano Lett. **12**, 1660 (2012).
[43] F. Pan, K. C. Smith, H. L. Nguyen, K. A. Knapper, D. J. Masiello, and R. H. Goldsmith, Elucidating energy pathways through simultaneous measurement of absorption and transmission in a coupled plasmonic-photonic cavity, Nano Lett. **20**, 50 (2020).
[44] A. D. McFarland, M. A. Young, J. A. Dieringer, and R. P. Van Duyne, Wavelength-scanned surface-enhanced Raman excitation spectroscopy, J. Phys. Chem. B **109**, 11279 (2005).
[45] Q. Quan and M. Lončar, Deterministic design of wavelength scale, ultra-high Q photonic crystal nanobeam cavities, Opt. Express **19**, 18529 (2011).